

# A multi-channel digital silicon photomultiplier array for nuclear medical imaging systems based on PET-MRI

Shingo Mandai<sup>†</sup> and Edoardo Charbon

## Abstract

We present a  $4 \times 4$  array of digital silicon photomultipliers (D-SiPMs) capable of timestamping up to 48 photons per D-SiPM and we show the advantage of generating multiple timestamps in the context of positron emission tomography (PET). The D-SiPMs have a pitch of  $800 \mu\text{m}$  and comprise 416 pixels each; the timing resolution achieved by the SiPMs is 179 ps FWHM, while each pixel has a fill factor of up to 57 % and a single-photon timing resolution of 114 ps.

## Introduction

A Silicon photomultiplier (SiPM) is an alternative to photomultiplier tubes (PMTs); it is often preferred to PMTs because of its tolerance to magnetic fields, compactness, and low bias voltage. At least two flavors exist for SiPMs: analog and digital. An analog SiPM (A-SiPM) consists of an array of avalanche photodiodes operating in Geiger mode, whose avalanche currents are summed in one node as shown in Fig. 1 (a) [1]–[6]. In a digital SiPM (D-SiPM), each photo-detecting cell or pixel consists of a single-photon avalanche diode (SPAD), whereas specific circuit elements are added to generate digital signals for each photon detection [7]. All of the SPAD outputs are combined together by means of a digital OR; see Fig. 1 (b). In most D-SiPMs, the global output is directly routed to an on-chip time-to-digital converter (TDC) to reduce external components and temporal noise. The disadvantage of D-SiPMs is the fact that only one optical photon or noise event determines the response of the sensor. Alternatively, the approach pursued in [8] can detect multiple photons and generate timestamps for each of them, by implementing a on-pixel TDC as shown in Fig. 1 (c), thus providing more detailed statistical information of the Gamma event in case of PET [8], [9]. However in this approach, the fill factor is low due to the use of a TDC per pixel. To increase fill factor while capturing multiple photon statistics, multiple pixels can share one TDC. Fig. 1 (d) [12] shows a case in which a column of SPADs shares one TDC, and the multiple timestamps can be utilized in a statistical approach for multiple-photon detection [11].

## Analysis of MD-SiPM for PET applications

In PET, one wants to detect the visible scintillation of a gamma photon when it interacts with a scintillating crystal. As shown in [10], [11], the most accurate time-of-interaction (TOI) is achieved by accounting for not one but several visible photons resulting from the scintillation. A multi-channel D-SiPM (MD-SiPM) was proposed in [12], [13] to generate several such timestamps from a scintillation event. The procedure for calculating the  $r$ th-order statistics and the Cramer-Rao bound for the unbiased estimator was demonstrated in [13]. In the analysis it was found that MD-SiPMs are more robust than their counterparts to noise and other

environmental conditions. Fig. 3 (a) and (b) show that the most accurate TOI is always guaranteed irrespective of the dark count rate (DCR) levels for a given illumination (assumed from a LYSO scintillator).

## Proposed SiPM architecture

Fig. 4 shows the proposed MD-SiPM array configuration. Each SiPM in the array comprises 416 pixel and measures  $800 \times 780 \mu\text{m}^2$ , adapted to the crystal dimensions. Each pixel measures  $50 \mu\text{m} \times 30 \mu\text{m}$ ; it generates a sharp pulse in correspondence to a photon detection that is routed directly to a TDC. Adjacent pixels are routed to independent TDCs by triples (every three pixel, the TDC is reused); this approach prevents closely striking photons to be missed, thereby reducing local saturation. There are 48 TDCs per SiPM column, each operating simultaneously with a LSB duration of 44 ps. The schematic of the pixel and the column-parallel TDC, and the TDC timing diagram are shown in Fig. 5, 6 and 7, respectively.

## Measurement Results

The sensor chip was fabricated on a  $0.35 \mu\text{m}$  CMOS process, the die size is  $4.22 \times 5.24 \text{ mm}^2$  as shown in Fig. 8. Fig. 9 (a) plots the cumulative DCR for 'D15' SiPM showing the DCR distribution of 416 SPADs for several excess bias voltages and temperatures. Masking pixels reduces both DCR and fill factor, and thus PDE, defined as  $PDP \times FF$ , where  $PDP$  is the photon detection probability and  $FF$  the fill factor. However, the reduction is not linear because some pixels have very high DCR compared to the median DCR value. This mechanism can be seen in Fig. 9 (b). The TDCs were fully characterized using an electrical input, yielding a single-shot timing uncertainty of 60 ps (FWHM). Fig. 10 shows the TDC characterization. The timing resolution of each SiPM was established optically in a TCSPC experiment. A single-SPAD timing jitter (FWHM) of 114 ps and the timing jitter of the entire SiPM (all 416 pixels) of 179 ps (FWHM) at 3.0 V excess bias was measured with internal TDCs (Fig 11). Table I summarizes the  $4 \times 4$  MD-SiPM specifications in relation with conventional SiPMs.

## Coincident timing resolution prediction

To predict the coincident timing resolution (CTR) based on the MD-SiPM architecture and measurement data shown in the previous subsections, we carried out simulations, whereas the timing jitter for a single photon of the detector is swept from 50 ps to 1 ns while the parameters of a LYSO scintillator are the same as in the previous section. Figure 13 (a) shows the relation between the timing information for a single photon and the predicted FWHM of CTR with various detected photon numbers at negligible DCR levels. According to the simulation results, the predicted CTR for the MD-SiPMs with 179 ps single photon timing jitter will be 260 ps and 183 ps for 500 and 1000 photons, respectively, by utilizing multiple timestamps. Figure 13 (b) shows the relation between the timing information for a single photon and the predicted FWHM of CTR with various DCR values and 1000

Shingo Mandai and Edoardo Charbon are with TU Delft, The Netherlands (<sup>†</sup>s.mandai@tudelft.nl, e.charbon@tudelft.nl) The research leading to these results has received funding from the European Union Seventh Framework Programme (FP7/ 2007-2013) under Grant Agreement n°256984. The authors would like to thank Vishwas Jain of TU Delft and Pierre Jarron of CERN. The authors are also grateful to Xilinx, Inc. for FPGA donations.

detected photons. As shown in the results, CTR utilizing multiple timestamps doesn't degrade due to DCR while CTR utilizing a single timestamp degrades when DCR reaches a certain threshold.

## REFERENCES

- [1] P. Buzhan, B. Dolgoshein, L. Filatov, A. Ilyin, V. Kantzerov, V. Kaplin, A. Karakash, F. Kayumov, S. Klemin, E. Popova, and S. Smirnov, *Silicon photomultiplier and its possible application*, *Nucl. Instrum. Methods Phys. Res. A* vol. 504 no.1-3, pp. 48–52, 2003.
- [2] A. G. Stewart, V. Saveliev, S. J. Bellis, D. J. Herbert, P. J. Hughes, and J. C. Jackson, *Performance of 1-mm<sup>2</sup> silicon phomultiplier*, *IEEE J. Quantum Electron.* vol. 44, no. 2, pp. 157–164, 2008.
- [3] N. Zorzi, M. Melchiorri, A. Piazza, C. Piemonte, and A. Tarolli, *Development of large-area silicon photomultiplier detectors for PET applications at FBK*, *Nucl. Instrum. Methods Phys. Res. A*, vol. 636, no. 1, pp. 208–213, 2010.
- [4] M. McClish, P. Dokhale, J. Christian, C. Stapels, E. Johnson, R. Robertson, and K. S. Shah, *Performance measurements of CMOS position sensitive solid-state photomultipliers*, *IEEE Trans. Nucl. Sci.*, vol. 57 no. 4, pp. 2280–2286, 2010.
- [5] M. Mazzillo, G. Condorelli, D. Sanfilippo, G. Valvo, B. Carbone, A. Piana, G. Fallica, A. Ronzhin, M. Demarteau, S. Los, and E. Ramberg, *Timing performances of large area silicon photomultipliers fabricated at STMicroelectronics*, *IEEE Trans. Nucl. Sci.* vol. 57 no. 4, pp. 2273–2279, 2010.
- [6] MPPC, <http://jp.hamamatsu.com>
- [7] T. Frach, G. Prescher, C. Degenhardt, R. de Gruyter, A. Schmitz, and R. Ballizany, R., *The digital silicon photomultiplier — Principle of operation and intrinsic detector performance*, *IEEE Nuclear Science Symposium Conference Record*, N28–5, 2009.
- [8] C. Veerappan, J. Richardson, R. Walker, D. U. Li, M. W. Fishburn, Y. Maruyama, D. Stoppa, F. Borghetti, M. Gersbach, R. K. Henderson, and E. Charbon, *A 160×128 single-photon image sensor with on-pixel 55ps 10b time-to-digital converter*, *IEEE ISSCC Dig. Tech. Papers*, pp. 312–314, 2011.
- [9] J.R. Meijlink; C. Veerappan; S. Seifert; D. Stoppa; R.K. Henderson; E. Charbon; D.R. Schaart; *First Measurement of Scintillation Photon Arrival Statistics Unsign a High-Granularity Solid-State Photosensor Enabling Time-Stamping of up to 20,480 Single Photons*, *IEEE Nuclear Science Symposium Conference Record*, pp. 2254–2257, 2011.
- [10] M. W. Fishburn and E. Charbon, *System trade-offs in gamma-ray detection utilizing SPAD arrays and scintillators*, *IEEE Trans. Nuc. Sci.*, vol. 57 no. 5, pp. 2549–2557, 2010.
- [11] S. Seifert, H. T. van Dam, and D. R. Schaart, *The lower bound on the timing resolution of scintillation detectors*, *Phys. Med. Biol.*, vol. 57, pp. 1797–1814, 2012.
- [12] S. Mandai and E. Charbon, *A Fully-Integrated 780 × 800 μm<sup>2</sup> Multi-Digital Silicon Photomultiplier With Column-parallel Time-to-Digital Converter*, in *Proc. IEEE ESSCIRC*, pp. 89–92, 2012.
- [13] S. Mandai and E. Charbon, *A Multi-Channel Digital SiPMs: Concept, Analysis and Implementation*, *IEEE Nuclear Science Symposium Conference Record*, N34–4, 2012.
- [14] J. Glodo, W. Moses, W. Higgins, E. van Loef, P. Wong, S. Derenzo, M. Weber, and K. Shah, *Effects of ce concentration on scintillation properties of labr3:ce*, *IEEE Trans. Nucl. Sci.*, vol. 52, no. 10, pp. 1805–1808, 2005.
- [15] S. Park, *On the asymptotic fisher information in order statistics*, *IMetrika* vol. 57, no. 1, pp. 71–80, 2003.
- [16] S. Mandai and E. Charbon, *A 128-Channel, 8.9-ps LSB, Column-Parallel Two-Stage TDC Based on Time Difference Amplification for Time-Resolved Imaging*, *IEEE Trans. Nucl. Sci.*, vol. 59, no. 5, pp. 2463–2470, 2012.

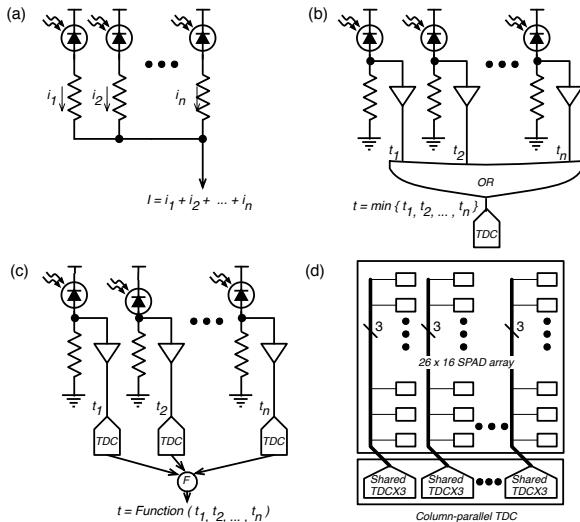


Fig. 1. The concept of (a) Analog SiPM, (b) conventional Digital SiPM, (c) Digital SiPM with on-pixel TDC and (d) Multi-channel Digital SiPM.

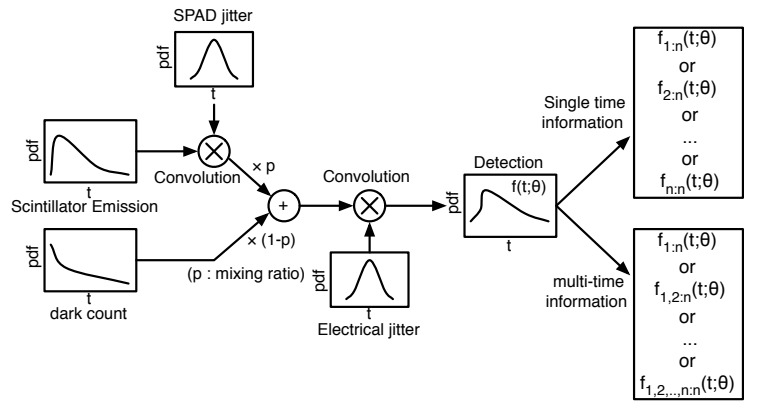


Fig. 2. Method for calculating the probability distribution function of the emission from a scintillator and DCR. For the emitted photons from a LYSO scintillator, we can assume that detection occurs at time,  $\theta$ . Time information of each photon can be considered as statistically independent and identically distributed (i.i.d) following a probability density function (pdf), which has been modeled as a double-exponential with rise time  $t_r$  and decay time  $t_d$  [14]  $f(t|\theta) = (\exp(-\frac{t-\theta}{t_d}) - \exp(-\frac{t-\theta}{t_r})) / (t_d - t_r)$  when  $t > \theta$ , otherwise,  $f(t|\theta) = 0$ . Upon photon impingement, the SPAD jitter and an electrical jitter are convolved with the scintillator-based pdf,  $f_{emi}(t|\theta)$ . The dark counts follow an exponential probability distribution with event rate,  $\lambda$ , and reset time,  $t_r$ , as  $f(t) = \lambda \exp(-\lambda(t - t_r))$  when  $t > t_r$ , otherwise,  $f(t) = 0$ . The pdf of the dark counts should also be convolved with electrical jitter to be  $f_{dcr}(t|t_r)$ . The detection cycle, or frame, starts at the earliest before  $\theta$  and it lasts a frame period,  $T$ . Thus the dark count pdf is summed up for each reset time and then normalized. The scintillator-based pdf and the dark count pdf are mixed with mixing ratio  $\alpha : (1 - \alpha)$  where  $\alpha$  is defined by the percentage of photons emitted from scintillator,  $N$ , out of total detectable events,  $N + \lambda T$ , as,  $f_{emi+dcr}(t|\theta) = \alpha f_{emi}(t|\theta) + (1 - \alpha) \frac{\int_{\theta-T}^{\theta} f_{dcr}(t|t_r) dt}{\int_{\theta-T}^{\theta} \int_{t_r}^{\infty} f_{dcr}(t|t_r) dt dr}$ .

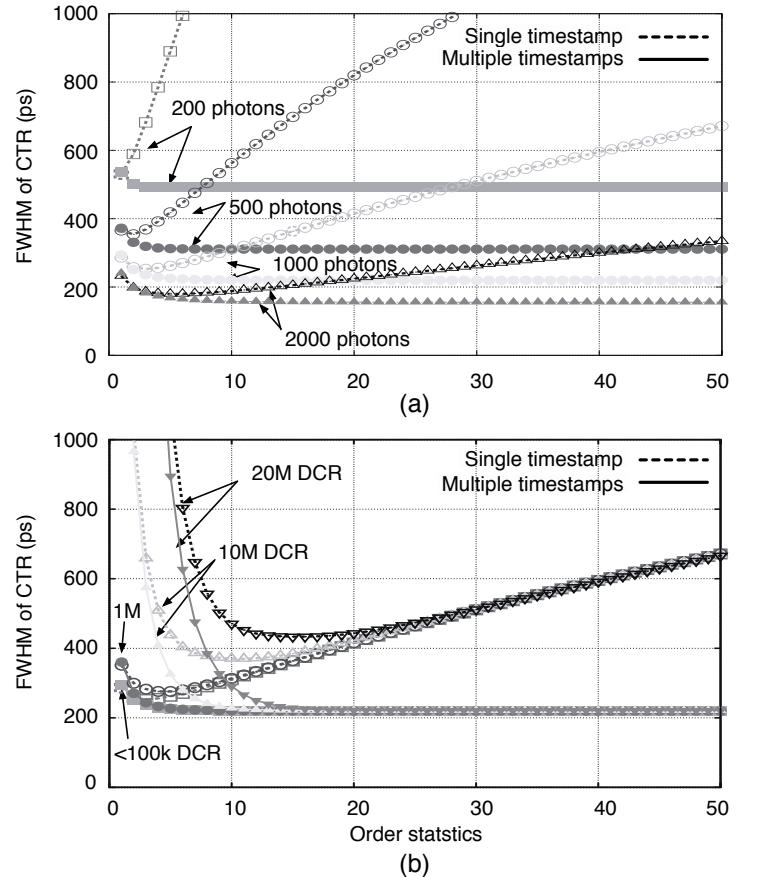


Fig. 3. Order statistics with a single timestamp or multiple timestamps v.s. FWHM of timing resolution assuming that normal SPAD jitter and electrical jitter distributions with a standard deviation of 100 ps, the rise and decay times of a LYSO scintillator are 200 ps and 40 ns, respectively (a) for a range of detected photon counts at 1 Hz DCR (which is almost negligible), (b) for a range of DCRs at 1000 detected photons.

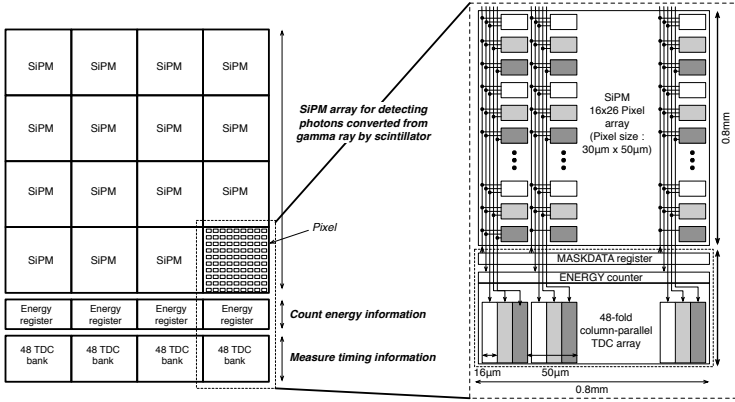


Fig. 4. Block diagram of the proposed sensor capable of detecting a large number of photons and their time-of-arrival with picosecond accuracy. The large number of TDCs enables to construct an accurate statistical profile for gamma photons.

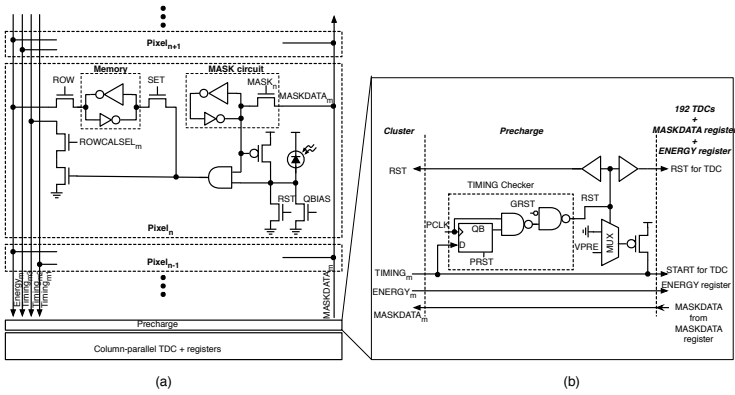
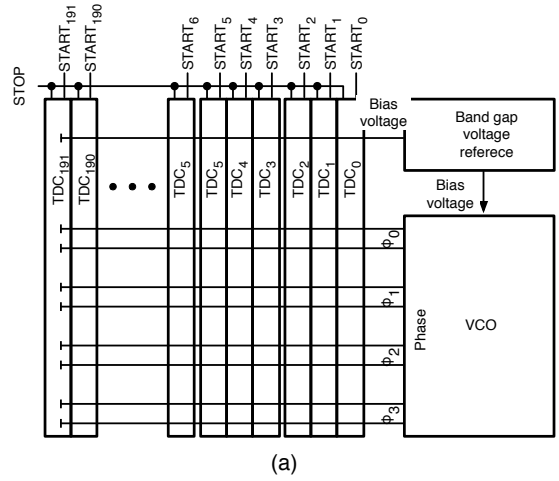
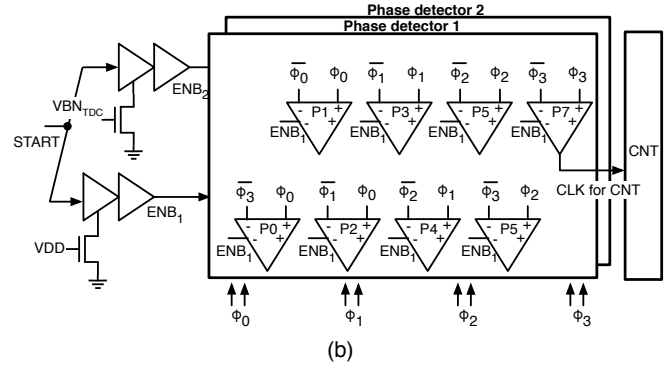


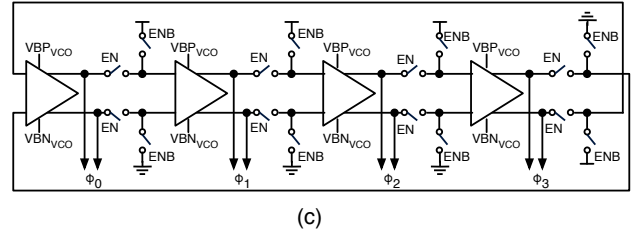
Fig. 5. (a) The pixel architecture comprises a SPAD, a 1-bit counter for energy estimation, a memory for masking, active and passive quenching, and a column driver circuit. The frame will start after control signal RST resets the SPAD. When a shower of photons is generated in the scintillator, one of them may hit the SPAD in the pixel, generating a digital pulse to pull-down  $TIMING_m$ . QBIAS controls the quenching resistance of the SPAD and also controls the digital pulse width to be more than the frame period. The event triggers the 1-bit counter, and it is read out as  $ENERGY_m$  by ROW after latching the 1-bit counter value by means of control signal SET. Masking is carried out in advance row-by-row, using signals  $MASKDATA_m$  and  $ROWCALSEL_m$ , by bringing the SPAD bias below breakdown and by disabling the signal generated at its anode. (b) Detail of the pre-charge structure implemented at the bottom of the array.  $TIMING_m$  is pre-charged during RST for pixels and TDCs and it occurs periodically every 6  $\mu s$  via signal GRST. PCLK is also causing pixels and TDCs to be reset when the number of firing TDCs is below a threshold within a pre-determined time, say 100 ns. This premature reset, known as *smart reset* is performed so as to prevent misses when TDCs are occupied by background photons or noise. VPRES is used for pull-up resistance for  $TIMING_m$ , and  $TIMING_m$  will be used as START for TDC.



(a)



(b)



(c)

Fig. 6. (a) VCO and reference circuit distributing 4 differential high-frequency phases to 192 TDCs. (b) Schematic of each TDC employing the phase interpolation technique. (c) VCO.

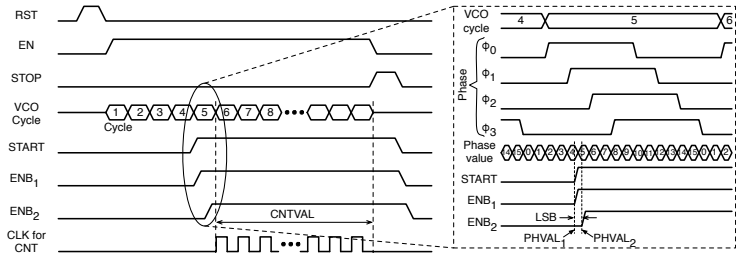


Fig. 7. Timing diagram. Two 4-bit phase information,  $PHVAL_1$  and  $PHVAL_2$ , are latched by  $ENB_1$  and  $ENB_2$ , and  $CNTVAL$  is stored as a coarse conversion result. By summing  $PHVAL_1$  and  $PHVAL_2$ , we obtain a fine conversion resolution of 5 bits (corresponding to a LSB of  $1.4 \text{ ns}/2^5 = 44 \text{ ps}$ ), which, added to the 12 bits of the coarse conversion, corresponds to a total of 17 bits. The final code is calculated as,  $CNTVAL \times 32 + (PHVAL_1 + PHVAL_2)$

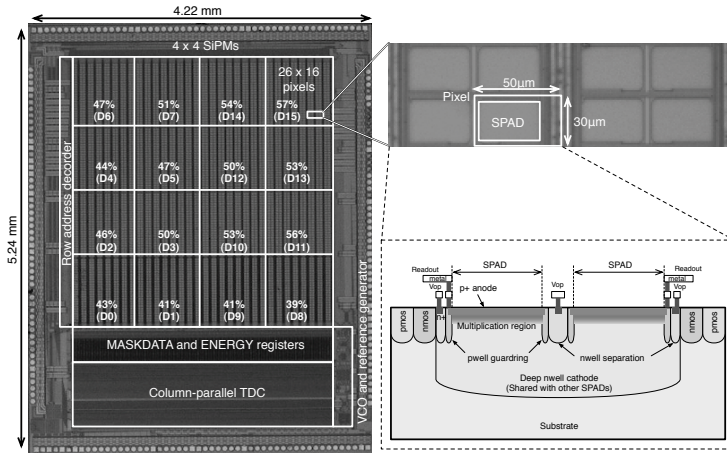


Fig. 8. Chip microphotograph. The chip occupies an area of  $22.1 \text{ mm}^2$  with a sensitive area of  $3.2 \times 3.2 \text{ mm}^2$ . It comprises an array of  $4 \times 4$  MD-SiPMs, implemented with a range of fill factors, from 39 to 57 %, as indicated in the figure. The cross-section and a detail of the pixels are also shown in the inset.

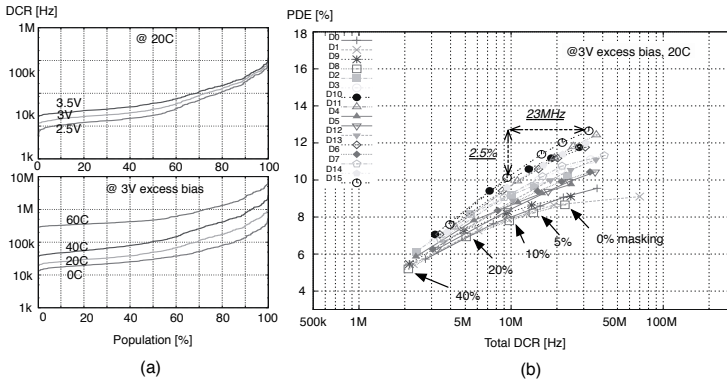


Fig. 9. (a) Cumulative DCR plot for various excess bias voltage and temperature conditions for the 'D15' SiPM. (b) Relation between DCR and PDE for various SiPMs at 3 V excess bias and  $20^\circ \text{C}$  for several masking levels, i.e. ratios of turned off pixels.

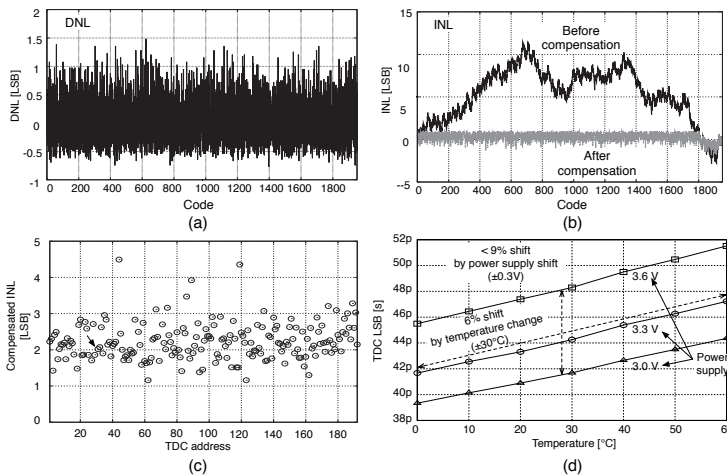


Fig. 10. (a) DNL. (b) INL. (c) INL before and after compensation in a TDC when all 192 TDCs are in operation. (d) LSB shift for the TDC due to temperature and power supply fluctuation. The TDCs suffer from a 6 % to 9 % LSB shift in the  $\pm 30^\circ \text{C}$  range and  $\pm 10\%$  power supply range.

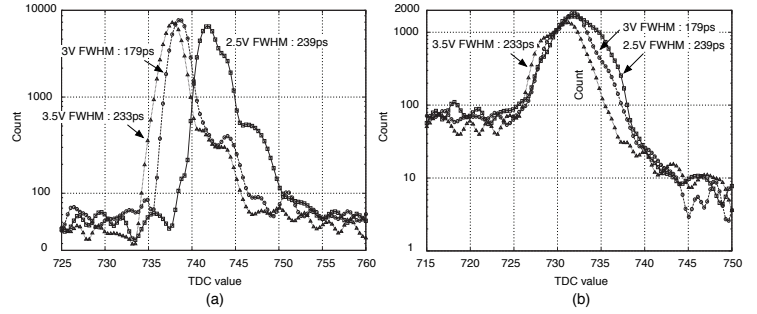


Fig. 11. The timing resolution of each SiPM was established optically in a TCSPC experiment using a 250 mW, 405 nm laser source (ALDS GmbH) with 40 ps pulse width and an external oscilloscope (LeCroy WaveMaster 6200). The TCSPC experiment was repeated using the internal TDCs operating at a nominal LSB of 44 ps. This measurement is the sum in quadrature of the contributions from the intrinsic jitter of the SPADs, TDCs, and sensor skews. (a) Single-photon FWHM timing resolution for a single SPAD using a TDC and an external oscilloscope. (b) Single-photon FWHM timing resolution for the complete SiPM at various excess bias voltages.

Parameter	This work	[5]	[6]	[7]	[8]	
Chip	Technology	0.35 $\mu\text{m}$ CMOS	Custom	Custom	0.18 $\mu\text{m}$ CMOS	
	# SiPMs	4 x 4	1	1	1	
	# SPAD / SiPM	416	4900	1600/400/100	6400	20480
TDC	SiPM Area	800 $\mu\text{m}$ x 780 $\mu\text{m}$	3.5mm x 3.5mm	1mm x 1mm	3.8mm x 3.3mm	8mm x 6.4mm
	# TDCs / SiPM column	48	-	-	2	20480
	# total TDC	192	Analog SiPM No TDCs	Analog SiPM No TDCs	2	20480
SPAD	Power / TDC (mA)	0.57 $\mu\text{A}$	-	-	-	-
	TDC LSB	44	-	-	24ps	55ps
	DCR ( $\text{Hz}/\mu\text{m}^2$ @ $20^\circ\text{C}$ )	39 @ $V_e=3.0\text{V}$	2.08	1.95/1.3/1.27	0.19	2 @ $V_e=0.73\text{V}$
SiPM	PDP at 420 nm (%)	30 @ $V_e=4.0\text{V}$	-	-	~60	22.5 @ $V_e=1.7\text{V}$
	Jitter (ps)	114 @ 405 nm	-	-	-	140 @ 637 nm
	FF (%)	57 (D15)	-	-	50	1
Timing resolution for blue light (single photon) (ps)	FF (%)	55.6	36	30.8/61.5/78.5	50	1
	Maximum PDE (%)	17 (D15)	-	25/50/65	15	-
	Total DCR (MHz)	10 ( $20^\circ\text{C}$ , 20% mask)	0.75	0.6/0.8/1	~2 ( $20^\circ\text{C}$ , 5% mask)	-
	Cross-talk (%)	< 10	-	Included in PDE	1	-
	Noisy pixels (%)	< 30	-	-	5	-
	Power [mW]	330 (16 SiPMs)	-	-	-	550
Timing resolution for blue light (single photon) (ps)	179 @ $V_e=3.0\text{V}$	164 @ $V_e=5.0\text{V}$	200-300	> 350**	280	

\* Including TDC arrays and readout circuit assuming all SiPMs are D15  
\*\* According authors' measurement and prediction

Fig. 12. Specification summary and comparison table. All the measurements are at room temperature unless otherwise specified. The major advantage of our sensor over conventional SiPMs with comparable fill factor is the flexibility and robustness given by the capability to establish multiple timestamps. This is especially important, considering the extreme environments in which the sensor is designed to operate.

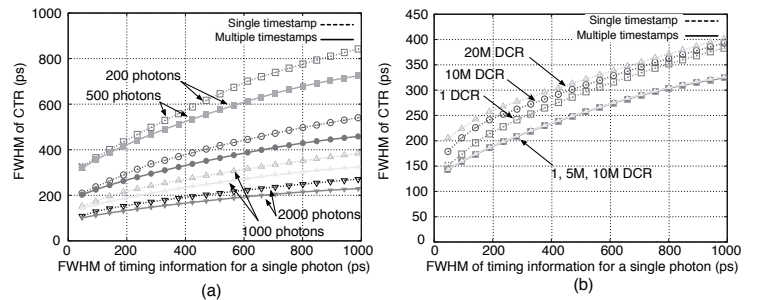


Fig. 13. Simulated FWHM of coincidence timing resolution (CTR) with a single timestamp and multiple timestamps: (a) for a range of detected photon numbers at 1 Hz DCR (which is almost negligible), (b) for a range of DCRs at 1000 detected photons.